where NA is the image-side numerical aperture of the projection lens.

According to our previously proposed quadratic aberration model (QAM) [20], the total aerial image intensity distribution can be expressed in the following formulation:

$$I(\mathbf{x}) \approx I_0(\mathbf{x}) + I_1(\mathbf{x}) + I_2(\mathbf{x}) = I_0(\mathbf{x}) + \sum_n Z_n I_{\text{lin}}^{(n)}(\mathbf{x}) + \sum_n \sum_m Z_n Z_m I_{\text{quad}}^{(n,m)}(\mathbf{x}), \tag{6}$$

where $I_0(\mathbf{x})$ is called the aberration-free intensity; $I_1(\mathbf{x})$ and $I_2(\mathbf{x})$ display the aberration-induced intensity distributions of linear and quadratic terms respectively. The $I_1(\mathbf{x})$ and $I_2(\mathbf{x})$ can be further decomposed into $I_{\text{lin}}^{(n)}(\mathbf{x})$ and $I_{\text{quad}}^{(n,m)}(\mathbf{x})$ multiplied by the corresponding Zernike coefficients, where $I_{\text{lin}}^{(n)}(\mathbf{x})$ and $I_{\text{quad}}^{(n,m)}(\mathbf{x})$ respectively represent the linearly and quadratically aberrated image terms based on individual Zernike aberrations. The $I_0(\mathbf{x})$, $I_{\text{lin}}^{(n)}(\mathbf{x})$, and $I_{\text{quad}}^{(n,m)}(\mathbf{x})$ are called the basis image terms, and can be directly calculated from $T_0(\mathbf{f}_1,\mathbf{f}_2)$, $T_{\text{lin}}^{(n)}(\mathbf{f}_1,\mathbf{f}_2)$, and $T_{\text{quad}}^{(n,m)}(\mathbf{f}_1,\mathbf{f}_2)$ by the formulations of

$$I_0(\mathbf{x}) = \iint O(\mathbf{f}_1)O^*(\mathbf{f}_2)T_0(\mathbf{f}_1,\mathbf{f}_2)\exp\left[-2\pi i(\mathbf{f}_1-\mathbf{f}_2)\cdot\mathbf{x}\right]d\mathbf{f}_1 d\mathbf{f}_2, \tag{7}$$

$$I_{\text{lin}}^{(n)}(\mathbf{x}) = \iint O(\mathbf{f}_1)O^*(\mathbf{f}_2)T_{\text{lin}}^{(n)}(\mathbf{f}_1,\mathbf{f}_2)\exp\left[-2\pi i(\mathbf{f}_1-\mathbf{f}_2)\cdot\mathbf{x}\right]d\mathbf{f}_1 d\mathbf{f}_2, \tag{8}$$

$$I_{\text{quad}}^{(n,m)}(\mathbf{x}) = \iint O(\mathbf{f}_1)O^*(\mathbf{f}_2)T_{\text{quad}}^{(n,m)}\exp\left[-2\pi i(\mathbf{f}_1-\mathbf{f}_2)\cdot\mathbf{x}\right]d\mathbf{f}_1 d\mathbf{f}_2. \tag{9}$$

Here $T_0(\mathbf{f}_1,\mathbf{f}_2)$, $T_{\text{lin}}^{(n)}(\mathbf{f}_1,\mathbf{f}_2)$, and $T_{\text{quad}}^{(n,m)}(\mathbf{f}_1,\mathbf{f}_2)$ are respectively called the aberration-free TCC, linearly aberrated TCC and quadratically aberrated TCC based on individual Zernike aberrations. Each term of $T_0(\mathbf{f}_1,\mathbf{f}_2)$, $T_{\text{lin}}^{(n)}(\mathbf{f}_1,\mathbf{f}_2)$, and $T_{\text{quad}}^{(n,m)}(\mathbf{f}_1,\mathbf{f}_2)$ can be represented as a weighted sum of several cross triple correlation (CTC) terms:

$$T_0(\mathbf{f}_1,\mathbf{f}_2) = C_{0,0;0,0}(\mathbf{f}_1,\mathbf{f}_2), \tag{10}$$

$$T_{\text{lin}}^{(n)}(\mathbf{f}_1,\mathbf{f}_2) = -ik\left[C_{n,0;0,0}(\mathbf{f}_1,\mathbf{f}_2) - C_{0,0;n,0}(\mathbf{f}_1,\mathbf{f}_2)\right], \tag{11}$$

$$T_{\text{quad}}^{(n,m)}(\mathbf{f}_1,\mathbf{f}_2) = -\frac{1}{2}k^2\left[C_{n,m;0,0}(\mathbf{f}_1,\mathbf{f}_2) - C_{n,0;m,0}(\mathbf{f}_1,\mathbf{f}_2) - C_{m,0;n,0}(\mathbf{f}_1,\mathbf{f}_2) + C_{0,0;n,m}(\mathbf{f}_1,\mathbf{f}_2)\right], \tag{12}$$

where $C_{k,l;m,n}(\mathbf{f}_1,\mathbf{f}_2)$ is a special CTC of the following notation with the definition $R_0(\mathbf{f}) = 1$:

$$C_{k,l;m,n}(\mathbf{f}_1,\mathbf{f}_2) = \int J(\mathbf{f})\left\{P(\mathbf{f}+\mathbf{f}_1)\left[R_k(\mathbf{f}+\mathbf{f}_1)\cdot R_l(\mathbf{f}+\mathbf{f}_1)\right]\right\}\left\{P^*(\mathbf{f}+\mathbf{f}_2)\left[R_m(\mathbf{f}+\mathbf{f}_2)\cdot R_n(\mathbf{f}+\mathbf{f}_2)\right]\right\}d\mathbf{f}. \tag{13}$$

The general form of CTC is defined as [22]:

$$\text{CTC}(\mathbf{f}_1,\mathbf{f}_2) = \int a(\mathbf{f})b(\mathbf{f}+\mathbf{f}_1)c(\mathbf{f}+\mathbf{f}_2)d\mathbf{f}, \tag{14}$$

where $a(\mathbf{f})$, $b(\mathbf{f})$, and $c(\mathbf{f})$ are three different functions.

It is noted that the final function $\text{CTC}(\mathbf{f}_1,\mathbf{f}_2)$ is four-dimensional and can be efficiently obtained by introducing the fast Fourier transform (FFT), which directly leads to a fast algorithm for the CTC calculation, therefore avoiding the time-consuming integration in Eqs. (13) and (14) [20]. It is also noted that each basis image terms of $I_0(\mathbf{x})$, $I_{\text{lin}}^{(n)}(\mathbf{x})$, and $I_{\text{quad}}^{(n,m)}(\mathbf{x})$ need to be calculated only once and then can be stored in advance for a given mask pattern. The total aerial image for the mask pattern can be quickly obtained by the weighted sum of these basis image terms multiplied by their corresponding Zernike terms. This property is particularly useful in the iterative procedure for retrieval of Zernike coefficients, as many iterations have to be performed and each iteration involves the calculation of several aerial images.

It is expected that the number of basis image terms, especially the number of quadratic terms shown in Eq. (9) is very large when all of the high order Zernike coefficients are taken

#166797 - $15.00 USD Received 16 Apr 2012; revised 31 May 2012; accepted 31 May 2012; published 12 Jun 2012
(C) 2012 OSA

into account. For example, when the lens aberrations need to be measured up to the 37th order, the number of quadratic terms is C_{37}^{2} = 666, which will lead to a large storage requirement and time-consuming aerial image calculations. Fortunately, some of the basis image terms shown in Eq. (9) are quite small due to the small value of their corresponding CTC terms shown in Eq. (12). Thus, it is possible to use many fewer basis image terms in the quadratic model, which will further reduce the storage requirement and computational intensity.

2.2 The iterative method for aberration measurement

Since the quadratic terms are taken into account in Eq. (6), it is not possible to establish a simplified model with a matrix of sensitivities to linearly relate the aerial image to the individual Zernike coefficients, which is the case for TAMIS, Z37 AIS and our previously proposed methods [6–10]. Here the aerial image is nonlinearly related to the individual Zernike coefficients as their interactions are considered. Therefore, the extraction of the Zernike coefficients becomes an inverse optimization problem as shown in Fig. 2, and an iterative procedure has to be performed to solve this problem.

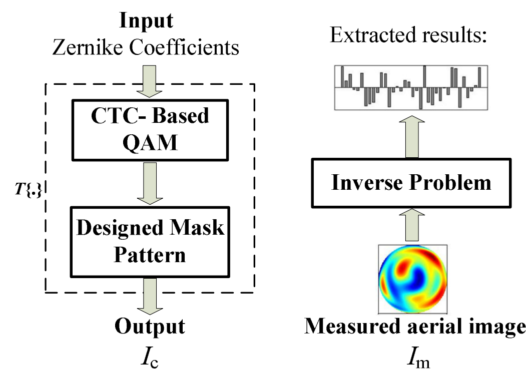

Fig. 2. Forward modeling and inverse problem for aberration measurement.

The CTC-based quadratic model provides a fast and accurate approach to represent the relationship between the Zernike coefficients and the aerial image intensity distribution. It could be utilized for aberration measurement by extracting the coefficients from the measured aerial image intensity. The flow of aberration measurement using the quadratic model is shown in Fig. 3, where the quadratic model is first established with the help of the CTC-based fast algorithm, which is the theoretical basis for efficiently simulating the through-focus series of aerial images.

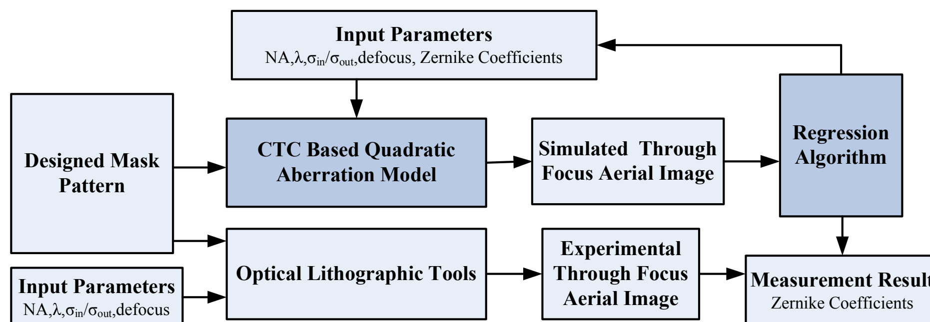

Fig. 3. The flowchart of the aberration measurement using the CTC-based quadratic aberration model. The Zernike coefficients are extracted by the regression algorithm from the experimental through-focus aerial images.

#166797 - $15.00 USD Received 16 Apr 2012; revised 31 May 2012; accepted 31 May 2012; published 12 Jun 2012
(C) 2012 OSA

Theoretically, any nonlinear regression methods such as local optimization algorithms can be used to solve the inverse problem for aberration measurement. The iteration process with the local optimization algorithm can be finished in several iterations, but it easily leads to only a local rather than a global solution. Therefore, we adopt the genetic algorithm to guarantee a global solution [23, 24], in which the Zernike coefficients are adjusted until the simulated aerial image intensity distribution fits the measured data. The optimization problem is formulated as follows:

$$\begin{aligned}\hat{\mathbf{Z}} &= \arg\min_{\mathbf{Z}} \sum_{k=1}^{N_h} \left| I_{\mathrm{m}}^{(h_k)}(\mathbf{x}) - T\{\mathbf{Z}\} \right| \\ &= \arg\min_{\mathbf{Z}} \sum_{k=1}^{N_h} \sum_{i=1}^{N_x} \sum_{j=1}^{N_y} \left| I_{\mathrm{m}}^{(h_k)}(x_i, y_j) - I_{\mathrm{c}}^{(h_k)}(x_i, y_j) \right|,\end{aligned} \tag{15}$$

where $\hat{\mathbf{Z}}$ represents the optimized vector of Zernike coefficients; $\mathbf{Z} = [Z_2, Z_3, \ldots, Z_N]$ represents the vector containing Zernike coefficients up to the Nth order; $I_{\mathrm{m}}^{(h_k)}(x_i, y_j)$ and $I_{\mathrm{c}}^{(h_k)}(x_i, y_j)$ respectively represent the measured and theoretical simulated aerial image at a coordinate of (x_i, y_j) and at a defocus of h_k; N_h indicates the number of defocus planes for aberration measurement; N_x and N_y indicate the number of image pixels in the x and y directions respectively. $T\{\cdot\}$ represents the forward modeling function transforming the Zernike coefficient vector $\mathbf{Z}$ into the theoretical simulated image, which can be calculated efficiently from Eq. (6).

3. Simulation

3.1 Simulation parameters

The lithographic simulator PROLITH was used to simulate the overall measurement performance by the proposed method. The simulations were performed on an HP Z800 Workstation of 3.46 GHz Opteron with MATLAB platform in a Windows 7 (64-bit) operating system. The optical system of the lithography tool was set as a partially coherent imaging system for a quadrupole source illumination with $\sigma_{\mathrm{out}} = 0.8$, $\sigma_{\mathrm{in}} = 0.4$, and degree = 45°. The wavelength used in the simulation is 193 nm, and the NA is 0.75. Figure 4 shows the aberrated wavefront values with Zernike coefficients from Z_2 up to Z_{37} that we used as inputs for simulation. The Zernike coefficients are random in the range of [-45mλ, 45mλ], leading to the aberrations in the range of [-150mλ, 150mλ], which are relatively very large.

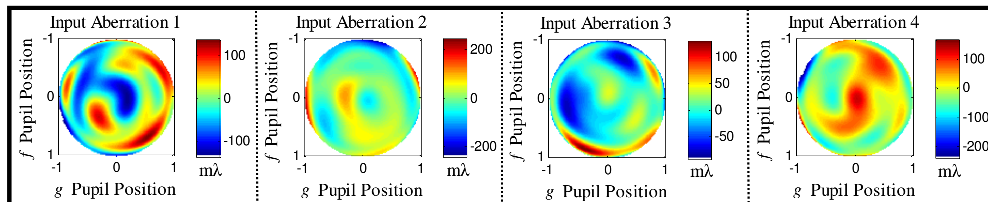

Fig. 4. Input values of aberrated wavefront for simulation.

As Zavyalova *et al.* have confirmed that the phase wheel target is highly sensitive to different types of aberrations [15–17], we utilized a similar input mask pattern but without phase shift shown in Fig. 5 as an example for the first demonstration of our aberration measurement method. The width of central contact is 600 nm while the width of all its surrounding contacts is 360 nm, and the simulation range of the mask pattern is [-1287 nm, 1287 nm].

#166797 - $15.00 USD Received 16 Apr 2012; revised 31 May 2012; accepted 31 May 2012; published 12 Jun 2012
(C) 2012 OSA

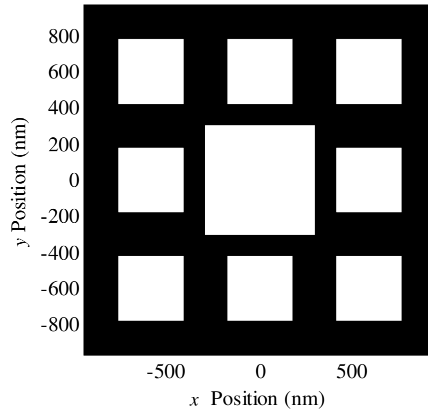

Fig. 5. The specially designed binary mask pattern for aberration measurement.

3.2 Aerial image calculations by the CTC-based quadratic aberration model

Figures 6 and 7 show the simulated linear terms and quadratic terms of odd aberrations (Z_7, Z_8) and even aberrations (Z_6, Z_9) respectively, for the test mask pattern shown in Fig. 5. It is noted that the linear terms of Z_6 and Z_9 are zero, and the quadratic terms, including $I_{\text{quad}}^{(6,7)}(\mathbf{x})$, $I_{\text{quad}}^{(6,8)}(\mathbf{x})$, $I_{\text{quad}}^{(7,9)}(\mathbf{x})$, and $I_{\text{quad}}^{(8,9)}(\mathbf{x})$, are extremely small. Thus, these terms will have no impact on the total aerial image intensity distribution, and can be eliminated from the aberration model.

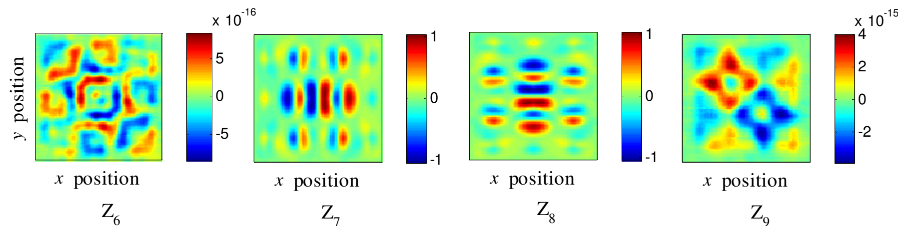

Fig. 6. The linear image terms of the mask pattern shown in Fig. 5 for Z_6, Z_7, Z_8, and Z_9.

It is also noted from Fig. 7 that the number of quadratic terms is very large when all of the high order Zernike coefficients are taken into account, which is expected from Eq. (9). For example, when the lens aberration needs to be measured up to the 37th order, the number of quadratic terms is 666. It is thus highly desirable to reduce the quadratic terms by omitting some of the terms that have no impact on the total aerial image. We performed simulations to establish the aberration model for 37th Zernike orders, so that the effect of individual Zernike term on the aerial image can be evaluated. The average aerial image intensity distribution was considered as the criterion to evaluate the impact on the total aerial image. As shown in Fig. 7, it is noted that the intercross terms between pairs of an odd Zernike coefficient and an even Zernike coefficient are small enough to be eliminated; hence, only the intercross terms between the same kinds of Zernike coefficients make sense. Therefore, it is possible to use many fewer quadratic terms in the quadratic model for total aerial image calculation. Based on the analysis of the simulations, the 666 quadratic terms can be reduced to 324 after eliminating those extremely small terms.

#166797 - $15.00 USD Received 16 Apr 2012; revised 31 May 2012; accepted 31 May 2012; published 12 Jun 2012
(C) 2012 OSA

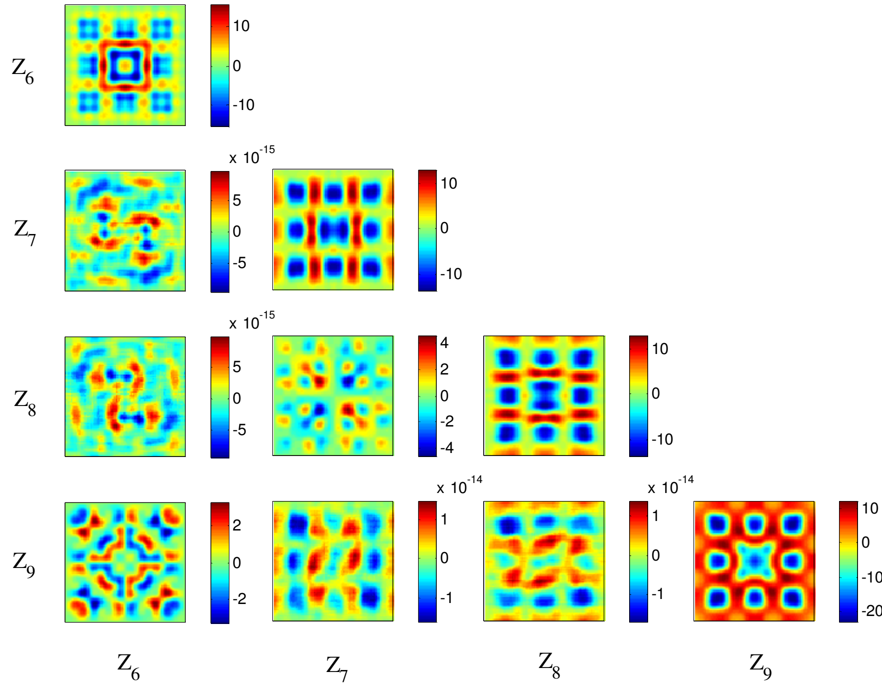

Fig. 7. The quadratic image terms of the mask pattern shown in Fig. 5 for intercross between pairs of Z_6, Z_7, Z_8, and Z_9.

Figure 8 depicts the aerial image calculation results for the test mask pattern shown in Fig. 5 with aberrations as Input Aberration 1 in Fig. 4. For the given mask pattern, the whole forward model took only 64.5 seconds to be built with an intensity error on the order 10^{-3} compared to that simulated by PROLITH. From this simulation and lots of other simulation results [20, 21], it is found that the proposed CTC-based quadratic model is suitable for fast and accurate aerial image calculations.

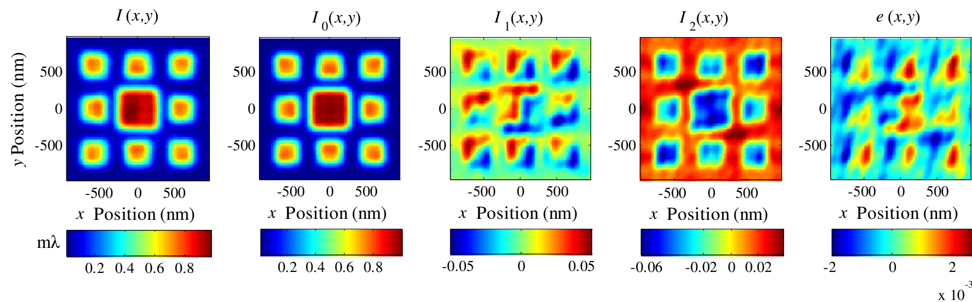

Fig. 8. Simulation results of the mask pattern shown in Fig. 5 for the Input Aberration 1 under the input parameters: NA = 0.75, λ = 193 nm, σ_{out} /σ_{in}/degree = 0.8/0.4/45°, and defocus = 0 nm.

3.3 Aberration measurement by the proposed iterative method

We then performed simulations of aberration measurement by solving the inverse optimization problem shown in Eq. (15), where the genetic algorithm was introduced for Zernike coefficients extraction. The experimental through-focus images were simulated by PROLITH at 3 defocus planes with defocus $h = -30$ nm, 0 nm, and 30 nm.

#166797 - $15.00 USD Received 16 Apr 2012; revised 31 May 2012; accepted 31 May 2012; published 12 Jun 2012
(C) 2012 OSA

Figure 9 shows the simulation result by the proposed method for the Input Aberration 1. The upper chart represents a comparison of the input Zernike coefficients with the measured values, and the lower chart represents the absolute errors of Zernike coefficients. The measured values of the Zernike coefficients are noted to coincide quite closely with the input values. From the simulation results, the absolute errors of all Zernike coefficients are less than 0.45mλ, and the root-mean-square of the absolute errors of Zernike coefficients up to Z_{37} is 0.14mλ.

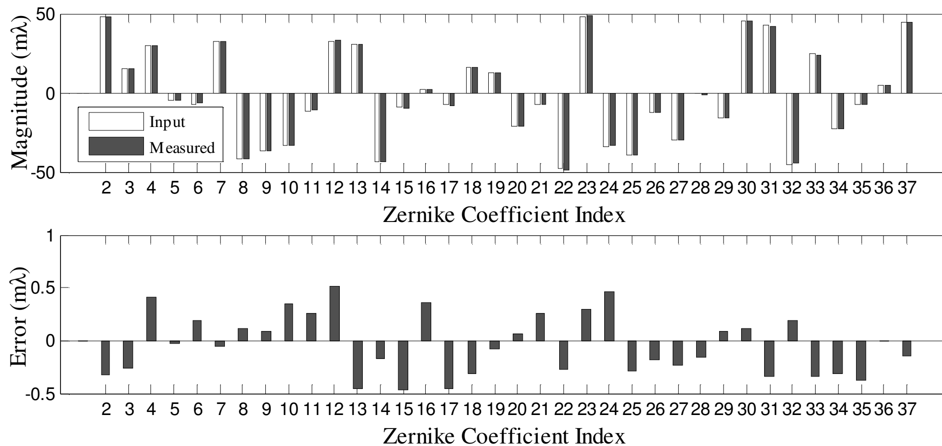

Fig. 9. Simulation result of aberration measurement for Zernike coefficients up to 37th order for the Input Aberration 1.

To test the accuracy of the proposed technique, all the aberrated wavefronts shown in Fig. 4 were inputed into the lithographic simulator for the simulated measurements of Zernike coefficients up to Z_{37}. Figure 10 shows the simulation result of the measurement errors of individual Zernike coefficients from Z_2 up to Z_{37}.

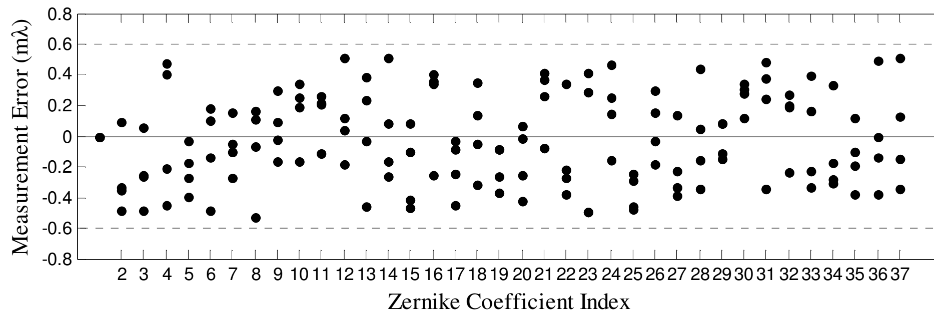

Fig. 10. Simulation result of the measurement errors of Zernike coefficients for all the input aberrated wavefronts.

As shown in Fig. 10, all the measurement errors of Zernike coefficients tend to be randomly distributed and converge within ± 0.6 mλ (or ± 0.116 nm), with the input aberration in the relatively large range of [-150mλ, 150mλ]. Furthermore, the agreement between the input and measured aberrated wavefronts is illustrated in Fig. 11. It is noted that the absolute measurement errors are less than 2.5 mλ (or 0.483 nm).

#166797 - $15.00 USD Received 16 Apr 2012; revised 31 May 2012; accepted 31 May 2012; published 12 Jun 2012
(C) 2012 OSA

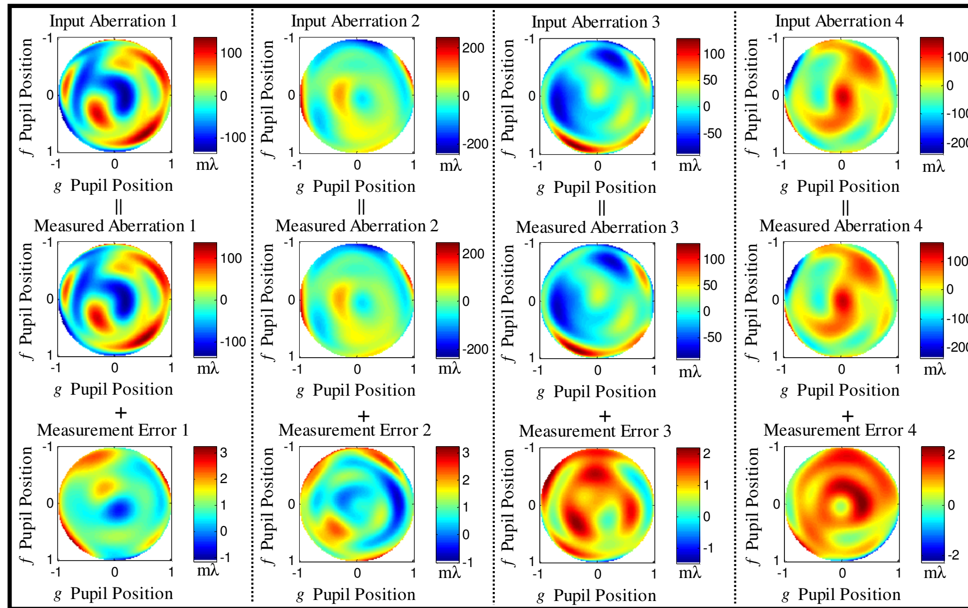

Fig. 11. Agreement between the input and measured aberrated wavefronts.

3.4 Comparison to the linear model method

We also performed a simulation to compare the measurement accuracy of the proposed iterative method using the quadratic model to the conventional method using the linear model. Recently, we reported a technique for *in situ* measurement of lens aberrations up to the 37th Zernike coefficient suitable for arbitrarily shaped illumination sources, and this technique has been demonstrated to outperform the widely used TAMIS and Z37 AIS techniques [9, 10]. With generalized formulations of odd and even aberration sensitivities, this technique is actually a simplified linear model method. Figure 12 shows the absolute measurement error of Zernike coefficients up to Z_{37} for different ranges of input aberrations, using both the proposed quadratic model and the simplified linear model.

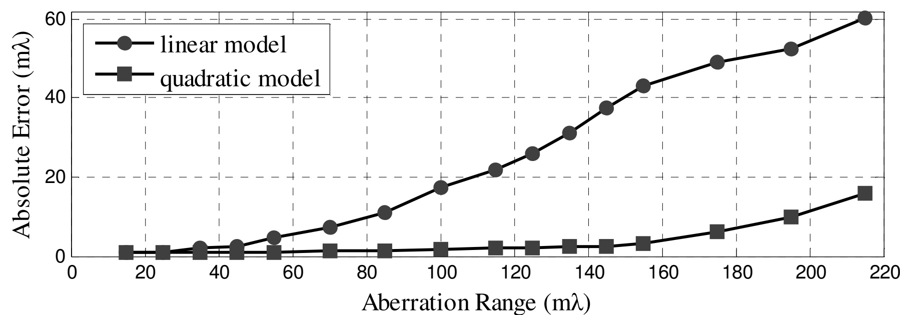

Fig. 12. Measurement accuracy by using the proposed quadratic model and the simplified linear model.

From Fig. 12, it is clear that both methods achieve a very good accuracy of wavefronts on the order of mλs when the input aberrations are small (less than 50 mλ). However, the measurement error when using the simplified linear model increases significantly as the aberration range increases, while that using the proposed quadratic model remains almost unchanged within the aberration range up to 160 mλ. This simulation demonstrates that the simplified linear model only works best only under the condition of small aberrations, while

#166797 - $15.00 USD Received 16 Apr 2012; revised 31 May 2012; accepted 31 May 2012; published 12 Jun 2012
(C) 2012 OSA

the proposed method significantly improves the measurement accuracy, particularly when the aberration is relatively large. This advantage of the proposed method is due to its further consideration of the quadratic terms.

4. Conclusion and future work

In this paper, we propose a method for *in situ* measurement of lens aberration in lithographic tools using a CTC-based quadratic model. By introducing the concept of CTC, the quadratic model can be calculated very quickly and accurately with the help of FFT. The Zernike coefficients up to the 37th order or even higher can be determined by solving an inverse problem through an iterative procedure with a genetic algorithm from several through-focus aerial images of a specially designed mask pattern.

Although capable of measuring aberrations up to the Z_{37} term, the widely used linear response model only works best under the condition of small aberrations. As the aberrations increase in size, the linear response model no longer maintains a high accuracy of wavefront estimates, because it ignores the interactions among individual Zernike aberrations. Using both theoretical analysis and simulation, the proposed method has overcome the significant drawback of the linear response model by further considering the quadratic terms.

Simulation results performed on a specially designed mask pattern has demonstrated that the proposed method is suitable for *in situ* measurement of Zernike coefficients up to the 37th order for a wide range of aberrations. It is particularly suitable for relatively large aberrations, with the measurement accuracy of Zernike coefficients on the order of 0.1 mλ (λ = 193 nm) and an accuracy of wavefronts on the order of mλs. The method also has the advantage of being simple to implement, and can be made to work in existing tools with no additional experimental setup.

It is worth pointing out that the sensitivity of the test mask pattern is critical for the aberration measurement, as the aberrations have unique characteristics in a manner that they influence specific portions of the lens pupil. For the purpose of aberration measurement, the mask pattern should be carefully designed so that it is most sensitive to particular aberration types and orders. With the fast algorithm of the CTC-based quadratic model, we will be able to perform the sensitivity analysis to optimize the mask pattern in our future work.

In the proposed method, the values of the effective source intensity distribution, defocus, and NA are all treated as known parameters that are inputed into the quadratic model for calculation of the theoretical aerial image. The measured aerial image should also be obtained so that the iterative process can be performed. For practical applications, however, all the input values of these parameters might be different from the real values in the lithographic tool, which means that all of these parameters might be error sources or uncertainty sources. To quantitatively evaluate the influence of these errors on the accuracy and precision of aberration measurement, we need to perform error analysis or uncertainty analysis, which is actually another important and challenging issue encountered in all kinds of inverse problems. We will deal with this issue together with experimental verification in our future work.

Acknowledgments

This work was funded by the National Natural Science Foundation of China (Grant No. 91023032, 51005091, 51121002), the National Science and Technology Major Project of China (Grant No. 2012ZX02701001), and the National Instrument Development Specific Project of China (Grant No. 2011YQ160002). The authors would like to thank the National Engineering Research Center for Lithographic Equipment of China for the support of this work and KLA-Tencor Corporation for providing an academic usage product of PROLITH™ software.

#166797 - $15.00 USD Received 16 Apr 2012; revised 31 May 2012; accepted 31 May 2012; published 12 Jun 2012
(C) 2012 OSA